EXHIBIT A

CONFIDENTIAL EXHIBIT

EXHIBIT B

ELSEVIER

Journal of Biomechanics 38 (2005) 1574–1581

JOURNAL OF BIOMECHANICS

www.elsevier.com/locate/jbiomech
www.JBiomech.com

Cardiovascular stent design and vessel stresses: a finite element analysis

C. Lally[a], F. Dolan[b], P.J. Prendergast[a,*]

[a]*Centre for Bioengineering, Department of Mechanical Engineering, Trinity College, Dublin 2, Ireland*
[b]*Medtronic Vascular, Parkmore Industrial Estate, Galway, Ireland*

Accepted 30 July 2004

Abstract

Intravascular stents of various designs are currently in use to restore patency in atherosclerotic coronary arteries and it has been found that different stents have different in-stent restenosis rates. It has been hypothesized that the level of vascular injury caused to a vessel by a stent determines the level of restenosis. Computational studies may be used to investigate the mechanical behaviour of stents and to determine the biomechanical interaction between the stent and the artery in a stenting procedure. In this paper, we test the hypothesis that two different stent designs will provoke different levels of stress within an atherosclerotic artery and hence cause different levels of vascular injury. The stents analysed using the finite-element method were the S7 (Medtronic AVE) and the NIR (Boston Scientific) stent designs. An analysis of the arterial wall stresses in the stented arteries indicates that the modular S7 stent design causes lower stress to an atherosclerotic vessel with a localized stenotic lesion compared to the slotted tube NIR design. These results correlate with observed clinical restenosis rates, which have found higher restenosis rates in the NIR compared with the S7 stent design. Therefore, the testing methodology outlined here is proposed as a pre-clinical testing tool, which could be used to compare and contrast existing stent designs and to develop novel stent designs.

Keywords: Coronary stent; Finite-element method; Restenosis; Vascular injury; Arterial-wall mechanics

1. Introduction

Many clinical studies have been carried out to investigate the performance of cardiovascular stents and it has been found that different stents have different in-stent restenosis rates (McClean and Eigler, 2002; Colombo et al., 2002) with in-stent restenosis found to occur in as many as 20–50% of stented vessels (Grewe et al., 2000). Numerous computational studies have been carried out to investigate the expansion and mechanical behaviour of different stent designs; both balloon-expanding stent designs (Dumoulin and Cochelin, 2000; Etave et al., 2001; Tan et al., 2001; Migliavacca et al., 2002; Chua et al., 2003; Petrini et al., 2004) and nitinol self-expanding stents (Whitcher, 1997). However, very few analyses have been performed on the interaction between the stent and the artery, even though vascular injury has been hypothesized as the stimulus for the formation of occlusive intimal hyperplasia and eventual restenosis (Edelman and Rogers, 1998). In fact, vascular injury caused to a vessel by the implantation of a stent, whether defined by the depth of penetration of the stent wires or by an aggressiveness score, has consistently been found to determine the degree of restenosis (Schwartz and Holmes, 1994; Arakawa et al., 1998; Hoffman et al., 1999) and restenosis is therefore strongly linked to stent design (Rogers and Edelman, 1995; Kastrati et al., 2000).

In recent years, drug-eluting stents have emerged as an alternative to bare metal stents and are coated in an

*Corresponding author. Tel.: +353-1-608-1383; fax: +353-1-679-5554.
E-mail address: pprender@tcd.ie (P.J. Prendergast).
URL: http://www.biomechanics.ie.

0021-9290/$ - see front matter © 2004 Elsevier Ltd. All rights reserved.
doi:10.1016/j.jbiomech.2004.07.022

anti-proliferative drug to prevent in-stent restenosis. Although, these stents have shown much promise it is still generally accepted that the optimal approach to coronary revascularization still lies in further developments in both stent design and drug-eluting stents (Lepor et al., 2002). Rogers et al. (1999) used the finite-element method to carry out a 2D analysis to investigate balloon–artery interactions during stent placement and showed that factors such as the balloon-inflation pressures, stent–strut openings and balloon compliance can influence the contact stresses between the balloon and the arterial tissue within the stent–struts and hence vessel injury. However, their study was limited to a 2D analysis and furthermore used linear elastic material properties to model the arterial tissue. A study of the arterial tissue within repeating units of different commercially available stent designs has been reported by Prendergast et al. (2003); they reported tissue prolapse and arterial wall stresses; however stent–artery contact was not simulated in that analysis nor were the models fully three dimensional (3D) in so far as only one repeating unit of each stent design was modelled. A fully 3D model has been developed by Auricchio et al. (2001) to look at an improvement to a stent design; however, the arterial tissue stresses were not reported. The most detailed numerical model to-date of a cardiovascular intervention is that by Holzapfel et al. (2002). They have developed a 3D model of a harvested cadaveric vessel using the finite-element method. The stresses induced within the vessel for a balloon angioplasty and a Palmaz–Schatz stenting procedure were determined. However, the localized stresses around the stent struts, i.e., the stresses most likely to provoke in-stent restenosis, were not computed and consequently it would not be possible to determine differences in the level of vascular injury as a function of stent design from their study.

In this paper, we test the hypothesis that two different stent designs will provoke different levels of stress in the vascular wall. The stents analysed were the S7 (Medtronic AVE, Minnesota, USA) and the NIR (Boston Scientific, Massachusetts, USA) stent designs. If this hypothesis is confirmed, and if the two stents also have significantly different restenosis rates, the study would support the use of computer-based finite-element analysis as a pre-clinical testing methodology to analyse the biomechanical attributes of cardiovascular stents.

2. Materials and methods

A finite-element analysis requires the geometry and material properties of the stent and blood vessel and appropriate loading conditions to simulate the stenting procedure, as described below. The finite-element software used was MSC Marc/Mentat (Santa Ana, CA, USA).

2.1. Model geometry

The 3D geometry of the repeatable units of the fully expanded 3.5 mm diameter NIR and S7 stents was determined using a coordinate measurement technique reported earlier (Prendergast et al., 2003). The thickness of the struts was 0.1 mm. Using the repeating unit geometry of each stent design, solid models of the full stents were generated. The solid models generated were of the stents in a planar state, i.e., the geometry of the stents if they were cut open longitudinally and flattened out. The stent solid models was then meshed and 'wrapped' into a cylindrical shape by transferring the nodal coordinates from a Cartesian coordinate system into a cylindrical coordinate system. In this way FE meshes were generated for each stent design as shown in Fig. 1. The two stent designs differed greatly; the NIR is a slotted tube laser-cut stent with 7 crowns whilst the S7 is a modular stent with a circular cross-section, 10 crowns and welded joints.

The atherosclerotic coronary artery was modelled as an idealized vessel and represented by a cylinder with outside diameter of 4 mm and had a localized crescent-shaped axisymmetric stenosis with minimum lumen diameter of 2 mm, see Fig. 2. The plaque corresponds to a maximum stenosis of 56% of the proximal and distal lumen cross-sectional area.

The adaptive meshing capability within Marc/Mentat was used in the models for the arterial tissue to allow the mesh to adapt and refine at contact areas. This enabled the elements in the region of highest stress gradients to subdivide and the finer mesh allowed for more accurate stress and strain evaluation in critical regions.

2.2. Material properties

The two materials of the artery wall, arterial tissue and stenotic plaque, were modelled using a 5-parameter third-order Mooney–Rivlin hyperelastic constitutive equation. This has been found to adequately describe the non-linear stress-strain relationship of elastic arterial tissue (Lally and Prendergast, 2003). The general polynomial form of the strain energy density function in terms of the strain invariants, given by Maurel et al. (1998) for an isotropic hyperelastic material is

$$W(I_1, I_2, I_3) = \sum_{i,j,k=0}^{\infty} a_{ijk}(I_1 - 3)^m(I_2 - 3)^n(I_3 - 3)^o,$$
$$a_{000} = 0, \quad (1)$$

where W is the strain-energy density function of the hyperelastic material, I_1, I_2 and I_3 are the strain invariants and a_{ijk} are the hyperelastic constants. If the

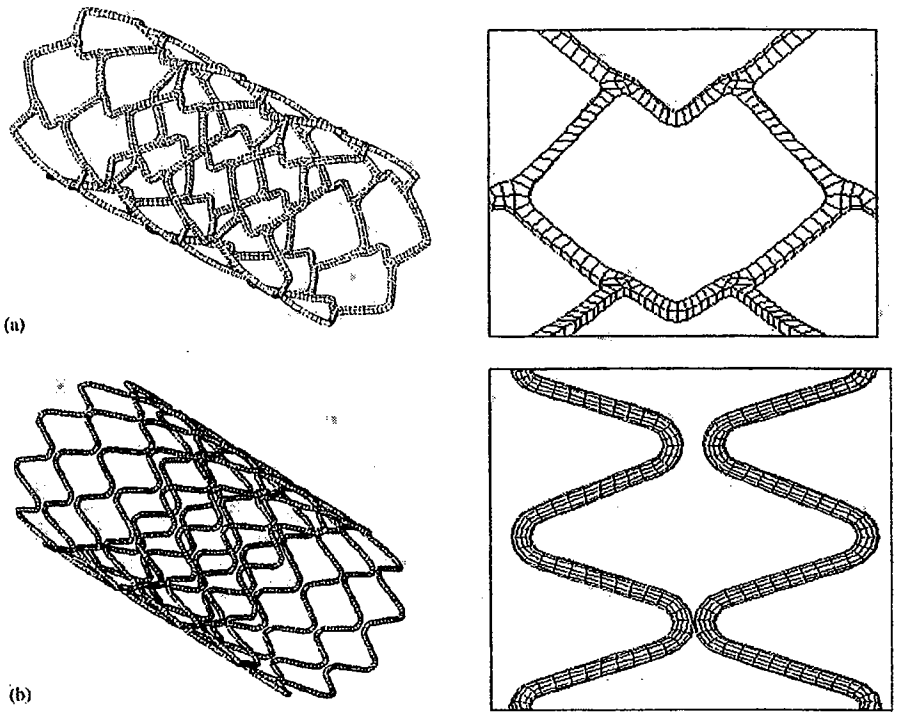

Fig. 1. Finite-element meshes of the fully expanded stents and exploded views of one repeating unit; (a) NIR stent and (b) S7.

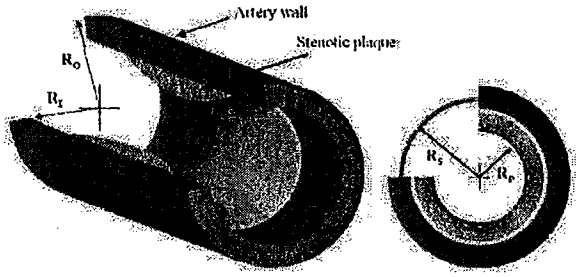

Fig. 2. Atherosclerotic coronary vessel geometry; artery outer radius, $R_0 = 2$ mm, Non-stenosed artery inner radius, $R_I = 1.5$ mm, stenosis inner radius, $R_P = 1$ mm, stent radius, $R_S = 1.75$ mm.

principal stretches of the material are denoted λ_1, λ_2 and λ_3, then the strain invariants for the material may be defined as

$$I_1 = \lambda_1^2 + \lambda_2^2 + \lambda_3^2, \tag{2a}$$

$$I_2 = \lambda_1^2\lambda_2^2 + \lambda_1^2\lambda_3^2 + \lambda_2^2\lambda_3^2, \tag{2b}$$

$$I_3 = \lambda_1^2\lambda_2^2\lambda_3^2. \tag{2c}$$

Arterial tissue may be taken as incompressible based on the results of previous studies (Carew et al.,1968; Dobrin and Rovick, 1969). $I_3 = 1$ for an incompressible material. The specific hyperelastic-constitutive model used to model the arterial tissue in this study is a specific form of Eq. (1) whereby the strain-energy density function is a third-order hyperelastic model suitable for an incompressible isotropic material and has the form given in Eq. (3) (Mooney, 1940).

$$W = a_{10}(I_1 - 3) + a_{01}(I_2 - 3) + a_{20}(I_1 - 3)^2 + a_{11}(I_1 - 3)(I_2 - 3) + a_{30}(I_1 - 3)^3, \tag{3}$$

Using Eq (3) the stress components can be obtained by differentiating the strain-energy density function, W, with respect to the corresponding strain components (Humphrey, 2002).

The arterial tissue material model was determined by fitting to data from uniaxial and equibiaxial tension tests of human femoral arterial tissue. The uniaxial and equibiaxial experimental and hyperelastic material model data are shown in Fig. 3. More details of the determination of the experimental data and this hyperelastic-material model are given in Prendergast et al. (2003). The hyperelastic constitutive model used to represent the plaque tissue in the vessel with a localized stenotic lesion was determined by fitting to published data for human calcified plaques (Loree et al., 1994), see Fig. 4. Table 1 summarizes the constants used for the hyperelastic constitutive equations to define the two material models. The stent material was modelled as linear elastic 316L stainless steel ($E = 200$ GPa, $\nu = 0.3$).

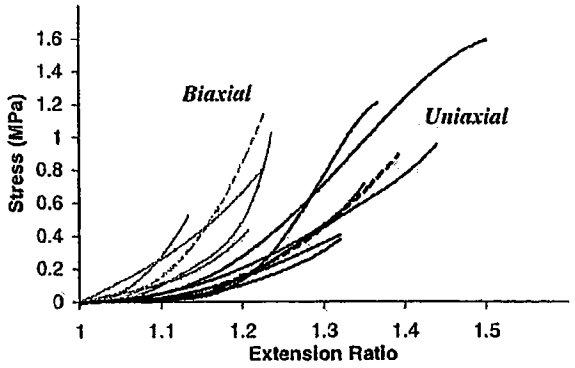

Fig. 3. Human femoral arterial tissue properties (solid lines) and the mechanical properties of the hyperelastic-material model for arterial tissue (dashed lines) (Prendergast et al., 2003).

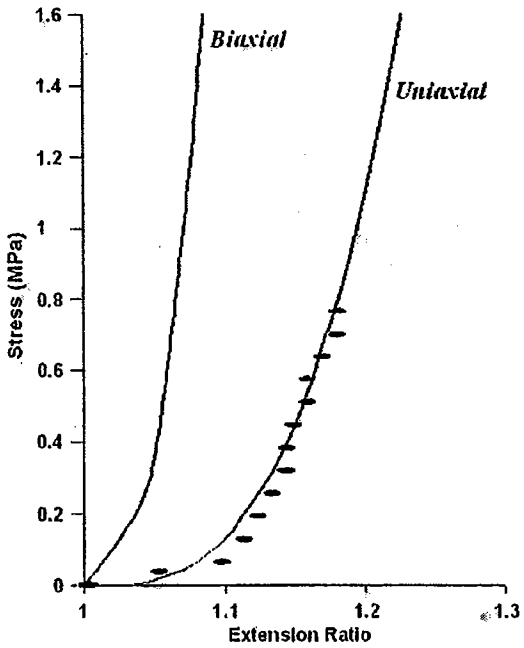

Fig. 4. Human calcified plaque properties (data points), adapted from Loree et al. (1994) (with permission), and the mechanical properties of the hyperelastic material model for plaque tissue (solid lines).

Table 1
Hyperelastic constants to describe the arterial tissue (Prendergast et al., 2003) and stenotic plaque non-linear elastic behaviour

	Arterial wall tissue (kPa)	Stenotic plaque tissue (kPa)
a_{10}	18.90	−495.96
a_{01}	2.75	506.61
a_{20}	85.72	1193.53
a_{11}	590.43	3637.80
a_{30}	0	4737.25

The parameters describe a Mooney–Rivlin model of the form given in Eq. (1).

2.3. Boundary conditions

The loading and restraint conditions were applied to the stent/artery construct in two steps. It involved use of the feature that exists in Marc/Mentat (and many other finite-element codes as well) that allows elements to be activated and deactivated during an analysis (called 'element birth and death'). In the first step, the stent elements were deactivated and the vessel was expanded to a diameter greater than that of the expanded stent by applying a sufficient internal pressure to the vessel (13 MPa). In the second step, the elements of the stent were activated and the pressure on the inner lumen of the artery was gradually reduced to a value of 13.3 kPa, corresponding to mean blood pressure of 100 mmHg. Due to the elastic nature of the hyperelastic arterial tissue the vessel contracted around the stent with the stent behaving as a scaffold within the vessel. Frictionless contact between the stent and the artery was assumed.

The contact algorithm implemented in marc/mentat was the direct constraint method. In this procedure, the motion of the bodies are tracked, and when contact occurs, direct constraints are placed on the motion using boundary conditions—both kinematic constraints on transformed degrees of freedom and nodal forces. Deformable–deformable contact was used to describe the contact between the two contact bodies, i.e., the stent and the artery. Both contact bodies were mathematically defined as analytical (NURB) surfaces. This leads to a more accurate solution because the normal to the contact surface is recalculated each iteration based upon the current surface position.

A longitudinal stretch of 1.2 was applied to the artery in an attempt to simulate the longitudinal tethering observed on coronary arteries in vivo (Weizsacker et al., 1983; Ogden and Schulze-Bauer, 2000). Axial restraints were applied to one end of the vessel. During the analysis the stent was restrained at one node in the circumferential direction to prevent rigid body rotations. Because of cyclic symmetry it was not necessary to model the entire stented vessel but rather only segments of the stented artery had to be modelled. Using the cyclic symmetry capability in Marc/Mentat, the nodes on the two cyclically symmetrical faces were coupled or tied. This allows out of plane motion (unlike planar symmetry constraints) and was therefore valid for representing a cyclically repeating segment of the stented vessel. Planar symmetry constraints cannot accurately model a cyclically repeating segment of a stenting procedure since the arterial geometry and the stent geometry in contact are not uniform in the axial direction. The NIR stent was represented by a cyclically repeating one-seventh segment whilst the S7 could only be represented by half-cyclic symmetry due to the position of the welds on the stent.

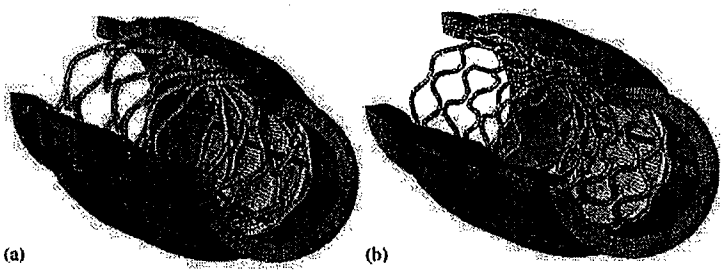

Fig. 5. The deformation of the artery, stenotic material and stent for (a) the NIR stent and (b) the S7 stent (one quarter of the artery and stenosis removed for viewing).

The element and node number used to represent the geometry of the two stenting simulations differed greatly as a result of the cyclic symmetry constraint applied. The one-seventh segment of the NIR stent was adequately represented by 125 elements and 470 nodes. For the half model of the S7, 5040 elements and 9021 nodes were necessary to model the circular cross-section of the stent. Although the mesh density used for the plaque and artery were the same in each model the number of elements differed since only one-seventh of the artery was represented in the NIR simulations whilst half of the artery had to be defined in the simulation of the S7 stenting procedure. This corresponded to 11,460 elements and 14,154 nodes for the NIR stenting procedure simulation and 40,040 elements and 47,783 nodes for the S7.

3. Results

The adaptive meshing incorporated into the simulations resulted in an increase in the number of elements and nodes defining the hyperelastic artery and plaque materials in both stenting simulations. The final number of elements that defined the artery was 22,072 (30,547 nodes) and 60,354 elements (80,293 nodes) in the NIR and S7 simulations, respectively.

The finite-element models predicted that both stents restored patency to the stenosed vessels, see Fig. 5a and b. As shown in Fig. 5a and b, the tissue drapes between the repeating units of the stents. Quantifying this, we find that the maximum tissue prolapse between the stent–struts to be 0.056 mm in the S7 stent compared with 0.124 mm for the NIR stent in the stenotic vessel. The contact area between the stent and the artery was 13.9 mm^2 for the NIR stent and 11.3 mm^2 the S7 stent.

The stresses induced within each stented vessel differed with a larger volume of highly stressed vascular wall predicted for the NIR stent, see Figs. 6 and 7. By analysing the volumes of the material stressed at different stress levels it was found that very high tensile stresses (>4 MPa) occurred in 21% of the artery stented with the NIR stent as compared to only 4% with the S7, see Fig. 7 for detailed results.

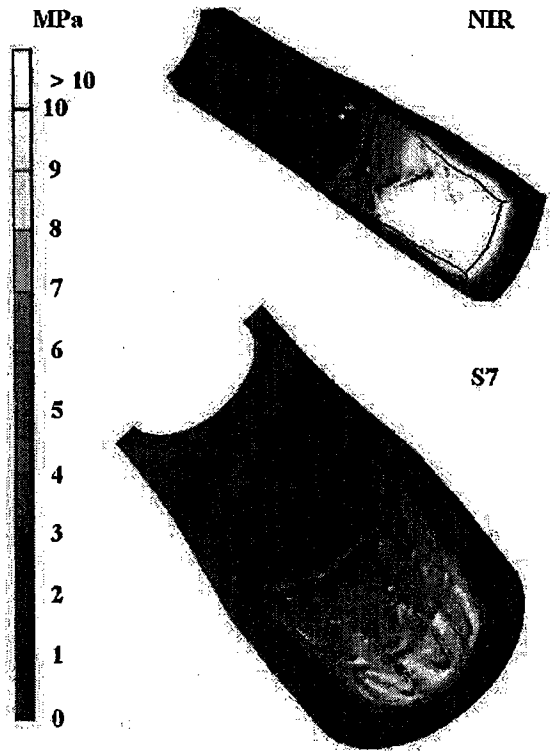

Fig. 6. Maximum principal stresses in atherosclerotic vessels stented with NIR and S7 stent. For symmetry reasons only 1/7 of the NIR and 1/2 of the S7 needs to be modelled.

Radial retraction was observed in the two stents as a result of the radial compressive forces exerted by the artery on the stents. This is to be expected due to bending of the stent struts and continued until equilibrium was reached between the radial strength of the stents and the radial compressive forces exerted by the artery. The retraction was found to be greater in the S7 compared with the NIR, see Fig. 8. The final lumen diameter corresponded to a final stenosis of 14% for the

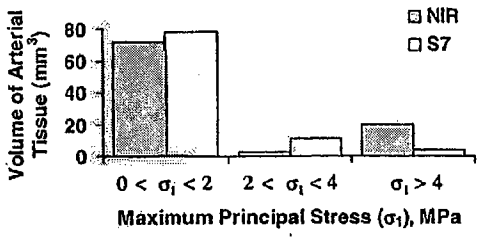

Fig. 7. Maximum principal stress volumes for the arterial tissue in the atherosclerotic vessel stented with an S7 and NIR stent.

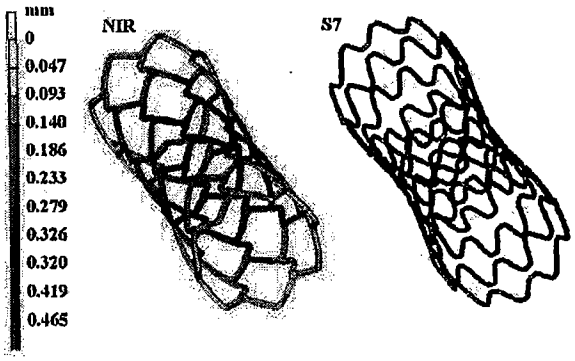

Fig. 8. Stent radial retraction in the models of the stented vessels.

NIR and 23% for the S7 stent, relative to the initial proximal and distal lumen area (i.e. the lumen area with a radius of 1.5 mm). However, the lumen cross-section was altered as a result of the axial stretch applied. As a result, the final lumen area at the stenosis corresponded to 8% increase in the lumen area, relative to the final proximal and distal lumen cross-sectional area in the NIR stenting simulation. It corresponded to 4% reduction (stenosis) in the final lumen cross-sectional area proximal and distal to the stenosis in the vessel stented with the S7 stent.

4. Discussion and conclusions

For a vessel with a localized stenotic lesion, based on the stresses induced in the vessel wall in these simulations, it is expected that the S7 would cause less vascular injury than the NIR. The lower volume of tissue stressed to high levels with the S7 stent compared to the same idealized geometry stented with the NIR made from the same material, can be attributed to the greater conformability of the S7 stent to the inner lumen geometry of the vessel. This includes the greater radial retraction observed in the S7 at the site of the vessel stenosis, see Fig. 8. By retracting, the stent maintains the lower stresses on the vessel; however the S7 maintains sufficient patency and superior scaffolding properties (0.056 mm maximum tissue prolapse compared with 0.124 mm for the NIR stent). In fact this value of maximum tissue prolapse is also very low compared with other stents designs (BeStent 2, *Medtronic AVE*; VELOCITY, *Cordis*; TETRA, *Guidant*), in which the maximum tissue prolapse within a repeatable stent unit of each of these designs has been determined in an earlier study (Prendergast et al., 2003).

Stent retraction is measured by the radial displacement of the stent; however, the tissue prolapse is tissue protrusion between the stent–struts and it defines the scaffolding properties of the stent. These results illustrate the coupling that exists between the stresses imposed on the vessel wall and the radial retraction of the stent. The radial retraction observed here is exaggerated as a result of the method used to simulate the stenting procedure, i.e., an expansion of the artery past the stent and the subsequent collapse of the artery around the stent. However, the simulations illustrate that if the two stent designs analysed were deployed using the same pressure in the same vessel that the NIR stent would induce higher stresses in the vessel wall. Clearly, an optimum stent design should retract sufficiently to prevent overstressing the vessel wall but still maintain patency of the vessel and plaque scaffolding. In fact, taking account of the differences in magnitude of radial retraction and tissue prolapse for the two stent designs, the minimum lumen diameter is predicted to be 2.63 and 2.79 mm at the vessel stenosis for the S7 and NIR stent, respectively. These correspond to 8% increase in the stenosis lumen area for the NIR stent and 4% reduction in the stenosis lumen area for the S7, relative to the final proximal and distal lumen area of the stented vessel. It is clear that the marginally higher lumen diameter achieved by the NIR stent is at the expense of large areas of considerably higher stress. These stresses may provoke a greater response to injury by the vessel wall and ultimately restenosis. This demonstrates the high risks associated with choosing an oversized rigid stent design as compared to the use of the more flexible S7 stent.

The clinical angiographic restenosis rate reported for the NIR stent is 19% at 6-month follow-up (Rutsch et al., 2000), and 19.3% at 9-month follow-up (Baim et al., 2001). The angiographic restenosis rate reported for the S7 stent at 6-month follow-up is 10.1% (Medtronic DISTANCE trial). The results of this study offer an explanation for this lower restenosis rate when compared with the NIR stent; the S7 stent would cause less vascular injury to the stented vessel and therefore would be expected to have a lower restenosis rate than the NIR stent whilst maintaining superior scaffolding properties than the NIR stent. It should also be noted that the S7 achieves high patency (only 4% stenosis) and excellent scaffolding whilst also having a lower stent/artery contact area (11.3 mm^2 as compared to 13.9 mm^2 for

the NIR). Maintaining the metal/tissue contact area low also reduces the thrombotic response of the vessel to the presence of a foreign material (Rogers and Edelman, 1995).

The main limitation of this study is that the arteries in which the stents are implanted are an idealized representation of stenosed coronary arteries. It is hypothesized, however, that the tortuosity of a realistic coronary artery model would only serve to further demonstrate the lower stresses generated by a flexible stent that can conform well to the vessel curvature relative to a stiffer stent. A more tortuous arterial geometry might also show that a rigid stent would cause even further high-stress concentrations and hence vascular injury at the ends of the stent, which could embed in the artery wall due to the relative non-conformability of the stent.

No rupture or damage mechanism has been incorporated into our plaque model. The high stresses observed in the calcified plaque are high enough that fracture could occur in this relatively brittle material. An analysis of the fracture process of the plaque is, however, beyond the scope of the present study. This study is currently being extended to develop a computational model of the restenosis mechanism using the stresses induced within the artery wall as a damage stimulus for the growth of restenotic tissue (Lally et al., 2004).

Finally, the process of stent expansion is not modelled in our simulations. This limits the study since it cannot be used to analyse the shearing force that an expanding stent could impose on an artery. In this respect, the approach used in this paper is suitable for studies that aim to look at the influence of stent placement on vessel wall stresses and stent-induced vascular injury after stent deployment since the stent geometry has been obtained from a stent in its expanded state.

The methodology described in this paper is proposed as a method to compare and analyse existing stent designs and can now also be used to develop new stent designs. Since this study already shows that stress predictions can be correlated with in-stent restenosis, it would be worthwhile to develop finite-element models of realistic vessel geometries, which can be obtained from Intravascular Ultrasound (IVUS) imaging. By determining full 3D patient specific geometries pre-stenting it may be possible to choose a stent design based on the patient's specific coronary artery stenosis geometry and thereby optimize the outcome of stenting procedures.

Acknowledgements

Project funded by an Applied Research Grant awarded by Enterprise Ireland to Medtronic Vascular, Galway, Ireland, and the Centre for Bioengineering, Trinity College, Dublin, Ireland, under the Programme for Research in Third Level Institutions, administered by the HEA.

References

Arakawa, K., Isoda, K., Sugiyabu, Y., Fukuda, M., Nishizawa, K., Shibuya, T., Nakamura, H., 1998. Intimal proliferation after stenting reflected by increased stent-to-vessel cross-sectional area ratio: serial intravascular ultrasound study. Journal of Cardiology 32, 379–389.

Auricchio, F., Di Loreto, M., Sacco, E., 2001. Finite-element analysis of a stenotic artery revascularization through a stent insertion. Computer Methods in Biomechanics and Biomedical Engineering 4, 249–263.

Baim, D.S., Cutlip, D.E., O'Shaughnessy, C.D., Hermiller, J.B., Kereiakes, D.J., Giambartolomei, A., Katz, S., Lansky, A.J., Fitzpatrick, M., Popma, J.J., Ho, K.K.L., Leon, M.B., Kuntz, R.E., NIRVANA Investigators, 2001. Final results of a randomized trial comparing the NIR stent to the Palmaz–Schatz stent for narrowings in native coronary arteries. American Journal of Cardiology 87, 152–156.

Carew, T.E., Vaishnav, R.N., Patel, D.J., 1968. Compressibility of the arterial wall. Circulation Research 22, 61–68.

Chua, S.N.D., MacDonald, B.J., Hashmi, M.S.J., 2003. Finite element simulation of stent and balloon interaction. Journal of Materials Processing Technology 143, 591–597.

Colombo, A., Stankovic, G., Moses, J.W., 2002. Selection of coronary stents. Journal of the American College of Cardiology 40, 1021–1033.

Dobrin, P.B., Rovick, A.A., 1969. Influence of vascular smooth muscle on contractile mechanics and elasticity of arteries. American Journal of Physiology 217, 1644–1651.

Dumoulin, C., Cochelin, B., 2000. Mechanical behaviour modelling of balloon-expandable stents. Journal of Biomechanics 33, 1461–1470.

Edelman, E.R., Rogers, C., 1998. Pathobiologic responses to stenting. American Journal of Cardiology 81, 4E–6E.

Etave, F., Finet, G., Boivin, M., Boyera, J.-C., Rioufol, G., Thollet, G., 2001. Mechanical properties of coronary stents determined by using finite element analysis. Journal of Biomechanics 34, 1065–1075.

Grewe, P.H., Deneke, T., Machraoui, A., Barmeyer, J., Muller, K.-M., 2000. Acute and chronic tissue response to coronary stent implantation: pathologic findings in human specimens. Journal of the American College of Cardiology 35, 157–163.

Hoffman, R., Mintz, G.S., Mehran, R., Kent, K.M., Pichard, A.D., Satler, L.F., Leon, M.B., 1999. Tissue proliferation within and surrounding Palmaz–Schatz stents is dependent on the aggressiveness of the stent implantation technique. American Journal of Cardiology 83, 1170–1174.

Holzapfel, G.A., Stadler, M., Schulze-Bauer, C.A.J., 2002. A layer-specific three-dimensional model for the simulation of balloon angioplasty using magnetic resonance imaging and mechanical testing. Annals of Biomedical Engineering 30, 753–767.

Humphrey, J.D., 2002. Cardiovascular Solid Mechanics. Cells, Tissues and Organs. Springer, New York.

Kastrati, A., Dirschinger, J., Boekstegers, P., Elezi, S., Schühlen, H., Pache, J., Steinbeck, G., Schmitt, C., Ulm, K., Neumann, F.-J., Schömig, A., 2000. Influence of stent design on 1-year outcome after coronary stent placement: a randomized comparison of five stent types in 1,147 unselected patients. Catheterization and Cardiovascular Interventions 50, 290–297.

Lally, C., Prendergast, P.J., 2003. An investigation into the applicability of a Mooney–Rivlin constitutive equation for modelling vascular tissue in cardiovascular stenting procedures. In:

Proceedings of the International Congress on Computational Biomechanics. Zaragoza, Spain, pp. 542–550.

Lally, C., Dolan, F., Prendergast, P.J., 2004. A computational model of in-stent restenosis in response to mechanical stress. In: Proceedings of the 10th Annual Conference of the Section of Bioengineering of the Royal Academy of Medicine in Ireland. Limerick, Ireland, p. 3.

Lepor, N.E., Madyoon, H., Kereiakes, D., 2002. Effective and efficient strategies for coronary revascularization in the drug-eluting stent era. Reviews in Cardiovascular Medicine 3, S38–S50.

Loree, H.M., Grodzinsky, A.J., Park, S.Y., Gibson, L.J., Lee, R.T., 1994. Static and circumferential tangential modulus of human atherosclerotic tissue. Journal of Biomechanics 27, 195–204.

Maurel, W., Wu, Y., Magnenat Thalmann, N., Thalmann, D., 1998. Biomechanical Models for Soft-Tissue Simulation. Springer, Berlin.

McClean, R., Eigler, N.L., 2002. Stent design: implications for restenosis. Reviews in Cardiovascular Medicine 3, S16–S22.

Medtronic DISTANCE trial: whitepaper reporting on the direct stenting with angiographic and clinical evaluation of the S7 (DISTANCE) trial: medtronic AVE, UC200203607EE 6M 5/02.

Migliavacca, F., Petrini, L., Colombo, M., Auricchio, F., Pietrabissa, R., 2002. Mechanical behavior of coronary stents investigated through the finite element method. Journal of Biomechanics 35, 803–811.

Mooney, M., 1940. A theory of large elastic deformation. Journal of Applied Physics 11, 582–592.

Ogden, R.W., Schulze-Bauer, C.A.J., 2000. Phenomenological and structural aspects of the mechanical response of arteries. In: Casey, J., Bao, G. (Eds.), Mechanics in Biology. BED 46, pp. 125–140.

Petrini, L., Migliavacca, F., Auricchio, F., Dubini, G., 2004. Numerical investigation of the intravascular coronary stent flexibility. Journal of Biomechanics 37, 495–501.

Prendergast, P.J., Lally, C., Daly, S., Reid, A.J., Lee, T.C., Quinn, D., Dolan, F., 2003. Analysis of prolapse in cardiovascular stents: a constitutive equation for vascular tissue and finite element modelling. ASME Journal of Biomechanical Engineering 125, 692–699.

Rogers, C., Edelman, E.R., 1995. Endovascular stent design dictates experimental restenosis and thrombosis. Circulation 91, 2995–3001.

Rogers, C., Tseng, D.Y., Squire, J.C., Edelman, E.R., 1999. Balloon–artery interactions during stent placement. A finite element analysis approach to pressure, compliance, and stent design as contributors to vascular injury. Circulation Research 84, 378–383.

Rutsch, W., Kiemeneij, F., Colombo, A., Macaya, C., Guermonprez, J.-L., Grip, L., Hamburger, J., Umans, V., Gotsman, M., Almagor, Y., Morice, M.-C., Garcia, E., Chevalier, B., Erbel, R., Cobaugh, M., Morel, M.-A., Serruys, P.W., 2000. Clinical and angiographic results with the NIR stent: First International NIR Endovascular Stent Study (FINESS-II). International Journal of Cardiovascular Interventions 3, 143–150.

Schwartz, R., Holmes, D.R., 1994. Pigs, dogs, baboons, and man; lessons in stenting from animal studies. Journal of Interventional Cardiology 7, 355–368.

Tan, L.B., Webb, D.C., Kormi, K., Al-Hassani, S.T.S., 2001. A method for investigating the mechanical properties of intracoronary stents using finite element numerical simulation. International Journal of Cardiology 78, 51–67.

Weizsacker, H.W., Lambert, H., Pascale, K., 1983. Analysis of the passive mechanical properties of rat carotid arteries. Journal of Biomechanics 16, 703–715.

Whitcher, F.D., 1997. Simulation of in vivo loading conditions of nitinol vascular stent structures. Computers and Structures 64, 1005–1011.